# Role of Curvature in Acridone for $^1O_2$ Oxidation of a Natural Product Homoallylic Alcohol: A Novel *Iso*-hydroperoxide Intermediate

Lloyd Lapoot,[1,2] Shakeela Jabeen,[1,3] Andrés M. Durantini,[1,4] and Alexander Greer[1-3]*

[1] Department of Chemistry, Brooklyn College, City University of New York, Brooklyn, New York 11210, United States

[2] Ph.D. Program in Biochemistry, The Graduate Center of the City University of New York, 365 Fifth Avenue, New York, New York 10016, United States

[3] Ph.D. Program in Chemistry, The Graduate Center of the City University of New York, 365 Fifth Avenue, New York, New York 10016, United States

[4] IDAS-CONICET, Departamento de Química, Facultad de Ciencias Exactas, Físico-Químicas y Naturales, Universidad Nacional de Río Cuarto, Ruta Nacional 36 Km 601, X5804BYA Río Cuarto, Córdoba, Argentina

Email address: agreer@brooklyn.cuny.edu

**Table of contents graphic**

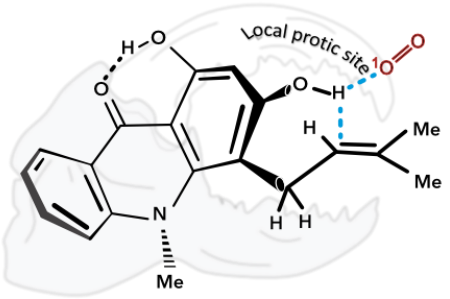


**Table of contents text**

Strategies for improving $^1O_2$ oxidation paths to dihydrobenzofurans are needed. A density functional theory study provides evidence that acridone curvature and phenol O–H···π bonding facilitate $^1O_2$ oxidation of a prenyl side-group to reach a dihydrobenzofuran. Mechanistic insight is provided for an *iso*-hydroperoxide intermediate preceding the dihydrobenzofuran. Notably, our evidence for the *iso*-hydroperoxide intermediate is reminiscent of other *iso* species, such as oxywater and *iso*-iodoform in fields outside of biosynthetic and $^1O_2$ chemistry.

**Abstract**

A density functional theoretical (DFT) study is presented, implicating a $^1O_2$ oxidation process to reach a dihydrobenzofuran from the reaction of the natural homoallylic alcohol, glycocitrine. Our results predict an interconversion between glycocitrine and an *iso*-hydroperoxide intermediate [R(H)$O^+$–$O^-$] that provides a key path in the chemistry which then

follows. Formations of allylic hydroperoxides are unlikely from a $^1O_2$ 'ene' reaction. Instead, the dihydrobenzofuran arises by $^1O_2$ oxidation facilitated by a 16° curvature of the glycocitrine ring imposed by a pyramidal *N*-methyl group. This curvature facilitates formation of the *iso*-hydroperoxide, which is analogous to the *iso* species $CH_2I^+–I^–$ and $CHI_2^+–I^–$ formed by UV photolysis of $CH_2I_2$ and $CHI_3$. The *iso*-hydroperoxide is also structurally reminiscent of carbonyl oxides ($R_2C=O^+–O^–$) formed in the reaction of carbenes and oxygen. Our DFT results point to intermolecular process, in which the *iso*-hydroperoxide's fate relates to O-transfer and $H_2O$ dehydration reactions for new insight to the biosynthesis of dihydrobenzofuran natural products.

**Introduction**

The biomimetic synthesis of dihydrobenzofuran has been reported in a singlet oxygen ($^1O_2$) oxidation of *o*-prenyl phenol **1** (Figure 1) (1). Products **2-5** were formed, where dihydrobenzofuran **2** was proposed to arise by H-bond interaction of phenolic hydrogen with $^1O_2$, directing it into the prenyl group. The formation of a peroxy intermediate was plausible, but evidence was not found in trapping experiments with triaryl phosphites. Because of our interest in the formation of natural product dihydrobenzofurans (2-5), we carried out a density functional theory (DFT) study to seek mechanistic insight into their formation.

Our DFT results indicate that prenyl phenol **1** bears a weaker internal hydrogen bond compared to glycocitrine **6** (Figure 2). As we will see, the curvature of glycocitrine **6** provides a stronger internal hydrogen bond thereby facilitating $^1O_2$ oxidation of the prenyl group by an *iso*-hydroperoxide intermediate. Notice the *iso* form [$R(H)O^+–O^–$] is zwitterionic (labeled as **11** in Figure 3), it is not the normal hydroperoxide form (ROOH). This difference is enforced because

of the hydroxy-directing interaction between the phenolic OH and $^1O_2$. The initial $^1O_2$-produced transition state appears to lead to the *iso* zwitterionic form. The special consequence is found from *iso*-hydroperoxide's appearance and downstream ability to form dihydrobenzofuran.

Here, we focus on glycocitrine **6** which is a *C*-prenylated phenol, bearing a 3-methylbut-2-enyl group on its acridone ring (6-8). Based on current understanding, this structure would be thought to favor the $^1O_2$ 'ene' reaction with formation of secondary and tertiary allylic hydroperoxides. The $^1O_2$ 'ene' has been reported for many homoallylic, *bis*- and *tris*-homoallylic alcohols (9-19), wherein our computational results point to ring curvature to enable a path to reach dihydrobenzofuran. In this way, the theoretical work allows us to predict a $^1O_2$ path that deviates from the 'ene' reaction. It involves a path to dihydrobenzofuran that extends beyond our experimental work (1).

Based on the DFT calculations, a proposed mechanism is shown in steps A to F (Figure 3). Conformational features of **6** in path A will be discussed first, followed by $^1O_2$ oxidation (path B), formation of an *iso*-hydroperoxide intermediate (path C), and subsequent paths D-F. As we mentioned above, a key facet of this study is the evidence for an *iso*-hydroperoxide intermediate. There are virtues in using DFT for insight into $^1O_2$ reactions (20-26). The formation of an *iso*-hydroperoxide intermediate is important in light of the existence of *iso* forms of hydrogen peroxide (oxywater, $H_2O^+O^-$) (27-29) and iodoform (*iso* $ICHI^+–I^-$) (30-33) as compared to their more stable forms, HOOH and $CHI_3$, respectively. Such *iso* species have been the subject of close examination in physical and organic chemistry. Here, for the first time, formation of an *iso*-hydroperoxide is implicated in a biosynthetic reaction, and this leads to the natural product dihydrobenzofuran, **9**.

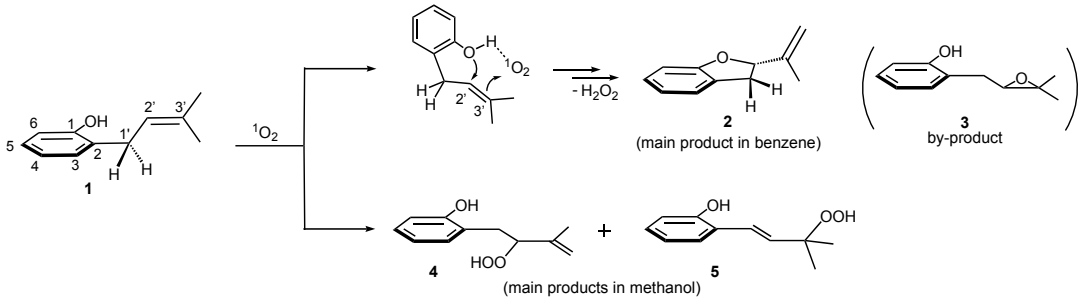


**Figure 1.** The sensitized photooxidation of *ortho*-prenyl phenol **1** in ref. 1. Preferential addition of $^1O_2$ to the prenyl site was attributed to hydrogen bonding with the phenol OH group, causing a divergence away from the singlet oxygen 'ene' products **4** and **5** toward the dihydrobenzofuran **2** as the major product in benzene.

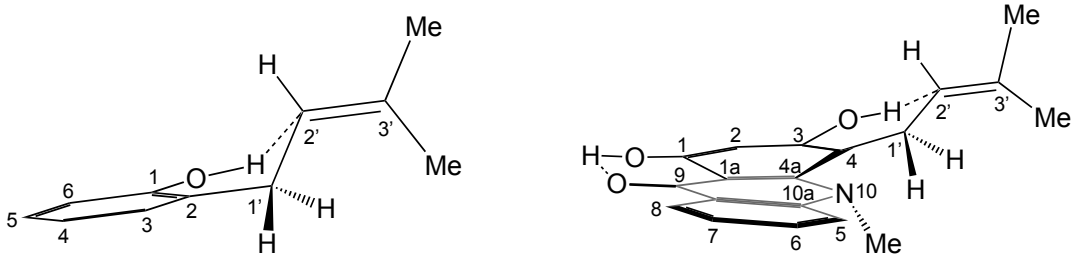

**1** **6**

**Figure 2.** Schematic drawing of prenyl phenol **1** showing a flat benzene ring and longer internal O–H···π bond. Glycocitrine **6** curvature distorts its phenol ring bringing the OH group and the prenyl group together closer.

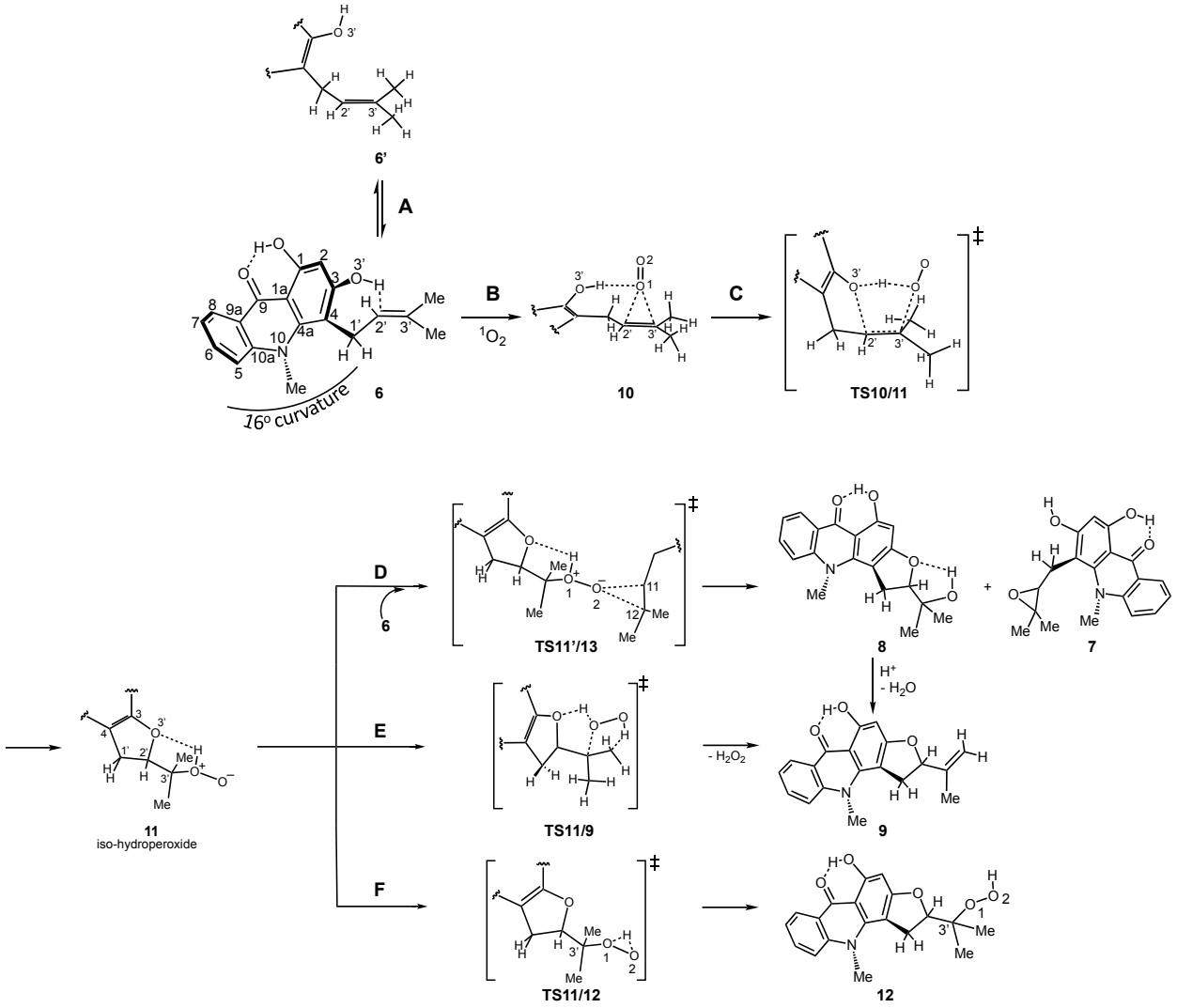


**Figure 3.** Proposed mechanism of $^1O_2$ oxidation of the prenyl group in the natural product glycocitrine **6**. Path A shows that the curved **6** accentuates an internal O–H···π bond [(*S*) amine shown; both stereoisomers accentuate this O–H···π bond]; path B is the $^1O_2$ oxidation and formation a H-bonded perepoxide **10**; path C is the formation of the *iso*-hydroperoxide **11**; path D is the epoxidation of another glycocitrine prenyl group by O-transfer from **11**; path E is formation of the dihydrobenzofuran **9** with the departure of $H_2O_2$; and path F is the rearrangement of the *iso*-hydroperoxide **11** to hydroperoxide **12**.

**Results and Discussion**

We now report the results of a DFT study that lead to the prediction for the existence of an *iso*-hydroperoxide intermediate. Described next are the computed conformations and distortions of glycocitrine **6** pertinent to $^1O_2$ oxidation, and computed routes via paths A-F accounting for the *iso*-hydroperoxide's formation and fate.

**Path A: Acridone Ring Curvature.** The B3LYP/D95(d,p) calculated structure for glycocitrine **6** shows curvature in it due to a distortion imposed by the pyramidal *N*-methyl group (Figure 4A). The computations show the formation of two conformations, **6** and **6b**, in which both display pyramidal character at nitrogen. In conformations **6** and **6b**, the fused rings possess dihedral angles C4–C4a–N10–C10a of 162.7° and C4–C4a–N10–C(Me) of -39.3° for **6**, and -163.9° and 35.5° for **6b**. Polycyclic aromatic hydrocarbons such as anthracene are flat with a dihedral angle of 180°. A transition structure is found to connect **6** and **6b** that is essentially planar with an activation energy of 7.1 kcal/mol. In glycocitrine, an *N*-methyl-induced distortion causes a scissor effect thereby strengthening an otherwise more remote and weaker O–H···π interaction. The deviation from planarity in the remote fused-rings in **6** enhances the O–H···π interaction of the phenol OH with the prenyl group as revealed by the calculations (Figure 4B). In **6**, notice the O3′–H group adopts a structure where H is positioned over the C2′ of the prenyl group; this leads to a stable conformation that has a dihedral angle (O3′–H–C2′–C3′) of -176.0°, H···C2′ distance of 2.028 Å, H···C3′ distance of 2.408 Å, and a O3′–H distance of 0.977 Å. In conformer **6b**, the dihedral angle (O3′–H–C2′–C3′) is -163.5°, the H···C2′ distance is 2.145 Å, and the H···C3′ distance is 2.490 Å, a O3′–H distance of 0.975, and a relative energy 0.8 kcal/mol below **6**.

Importantly, the H···C3′ bond distance in **6** and **6b** is decreased for a stronger O–H···π bond contribution in the reaction of glycocitrine **6** with $^1O_2$.

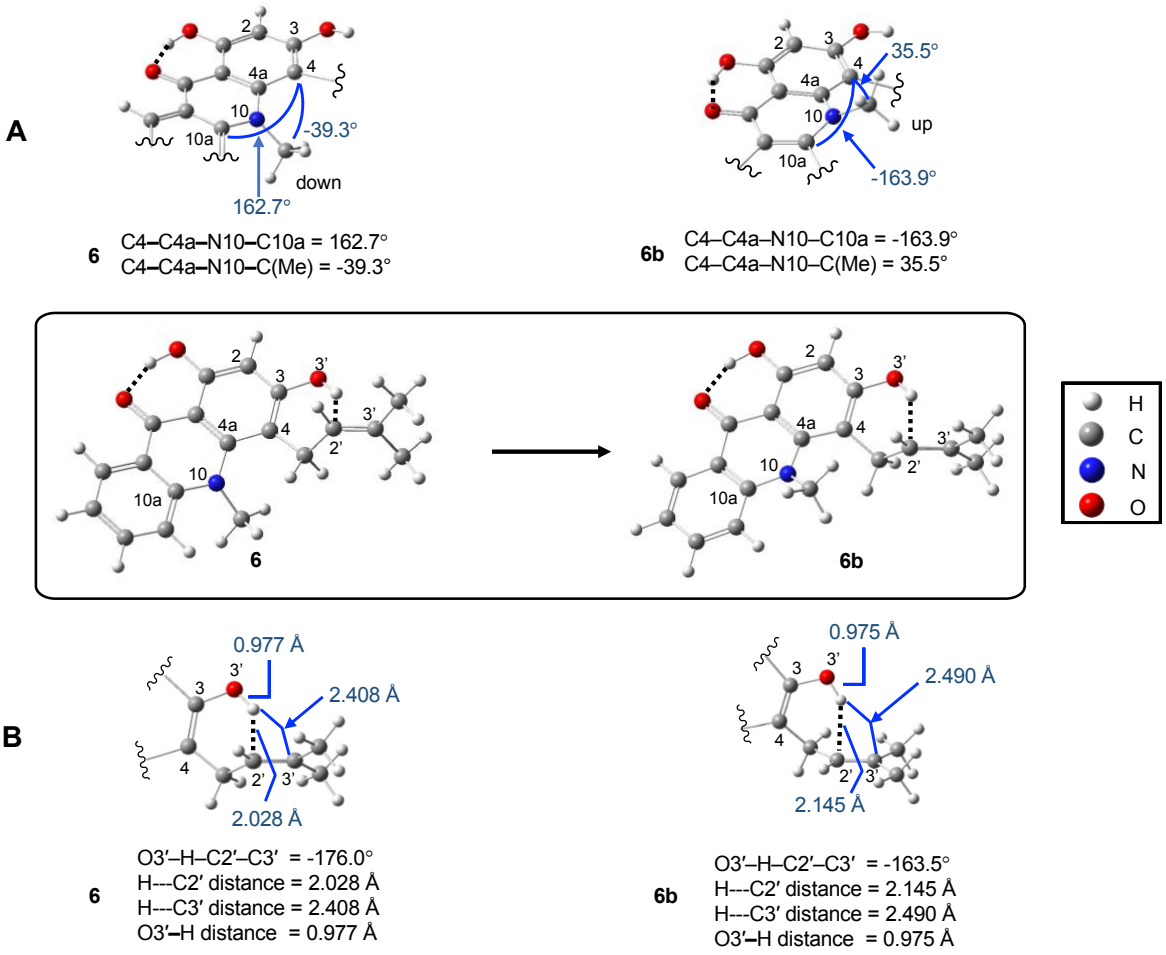


**Figure 4.** B3LYP/D95(d,p) optimized structures showing (A) the positions of the NMe group in **6** and **6b** as down and up, respectively, and (B) the soft O–H···π interaction of the phenol OH with the prenyl group in **6** and rotamer **6b**.

**Path B: $^1O_2$ Oxidation of the Prenyl Site Nearby an Alcohol Substituent.** Figure 5 shows that glycocitrine **6** contains a phenol O–H···π bond with the prenyl C2′=C3′ group. The hydrogen of O3′–H is located nearby at a H···C2′ distance of 2.028 Å for **6**, for an O–H···π interaction of 2.1 kcal/mol. Constrained optimizations predict an approach of $^1O_2$ to the prenyl site of **6** to reach an unsymmetrical perepoxide **10**. This perepoxide **10** is in a shallow minimum stabilized by 5.1 kcal/mol with B3LYP/D95(d,p) calculations and 8.9 kcal/mol with M062X/6-31+G(d,p) calculations (compared to the absence of the hydrogen bond, in which a transition structure C=C(π)···$^1O_2$ for **10** emerges). The phenol OH forms a H-bond to the unsymmetrical perepoxide **10** with an O1–C2′ bond distance of 2.114 Å, an O1–C3′ bond distance of 2.186 Å, and an O–H···O1 bond angle of 167.0°. Similarly, Adam et al. noted a steering effect by an amino group in the $^1O_2$ ene reaction of chiral allylic amines to assist $^1O_2$ attack (18). More detail on the hydrogen bonding of $^1O_2$ to the phenol OH was collected with NBO calculations. Figure 6 shows the results of NBO calculations with oxygen atom (O1) lone pair electrons (*lp1* and *lp2*) interacting with the σ* orbital of the phenol O3′–H; these donor-acceptor interactions were found to provide 10.52 and 1.43 kcal/mol stabilization, respectively, for a net energy of 11.95 kcal/mol. By comparison, the interaction of oxygen atom (O2) *lp1* and *lp2* with the σ* orbital of the phenol O3′–H were trivial, which is consistent with the shorter O3′–H···O1 bond distance (1.97 Å) relative to the O3′–H···O2 bond distance of 2.50 Å in **10**.

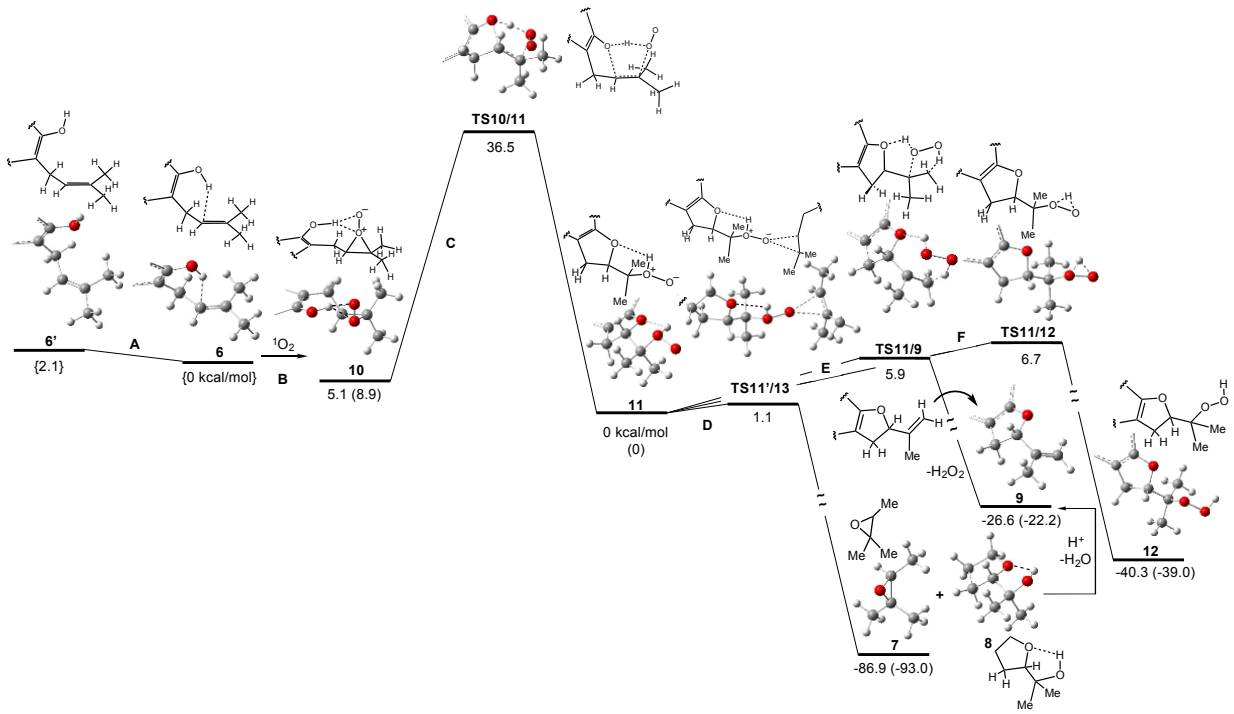


**Figure 5.** DFT calculated potential energy surface for the reaction of glycocitrine **6** with $^1O_2$. Gas-phase energetics are in kcal/mol, shown for B3LYP/D95(d,p), and in parentheses for M062X/6-31+G(d,p). Relative energies: **6** and **6′** are relative to each other; 2-(tetrahydrofuran-2-yl)propan-2-*iso*-hydroperoxide **11′** and 2-methyl-2-butene is relative to **7** and **8**; and **9** and **12** are relative to **11**.

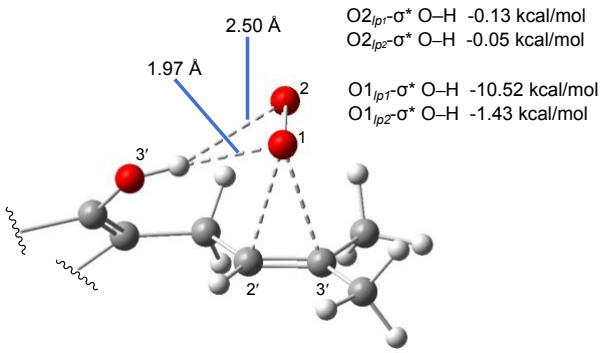


**Figure 6.** M062X/6-31+G(d,p) computed structure of the phenol OH stabilizing incoming $^1O_2$ to the prenyl site of **6**. NBO analysis of the oxygen atoms (O1 and O2) lone pair electron ($lp_1$ and $lp_2$) interactions with the σ* antibonding orbital of the phenol O3′–H group.

**Path C: Perepoxide Pirouette to Form *Iso*-hydroperoxide.** *The iso-hydroperoxide **11** is an intermediate supported by theoretical evidence.* Figures 5 and 7 show the formation of **11** by a O1=O2 pirouette motion that is accompanied by a decrease of the O1–C3′ bond distance. The O1=O2 relative to the C2′=C3′ bond in **10** is close-to-perpendicular with C2′–C3′–O1–O2 of -99.4°, which rotates counterclockwise via **TS10/11** C2′–C3′–O1–O2 of -118.9°, to a nearly linear orientation of *iso*-hydroperoxide's C2′–C3′–O1–O2 of -175.6°. Transition structure **TS10/11** is found which connects **10** and **11** with an activation energy of 30.9 kcal/mol. This oxygen pirouette movement to reach **11** is somewhat reminiscent of reported aryl vs alkyl ring pirouettes leading to anthracene and phenanthrene (34). A key facet is the computed preference for attachment of singlet oxygen's O1 for C3′. In **11**, the O1–C3′ bond distance (1.513 Å) is much shorter than the O1–C2′ bond distance (2.376 Å). Thus, there is intramolecular H-bonding assistance, e.g., bringing O1···C3′ bond closer (2.126 Å) in **TS10/11** in the conversion to **11**. The H-bond between

hydrofuran oxygen O and H helps to stabilize the *iso* form of **11** against deprotonation. To determine the factors that underlie **11** interconversion, three mechanistic pathways were examined. One arises from a bimolecular reaction (path D), and two others from unimolecular reactions (paths E and F).

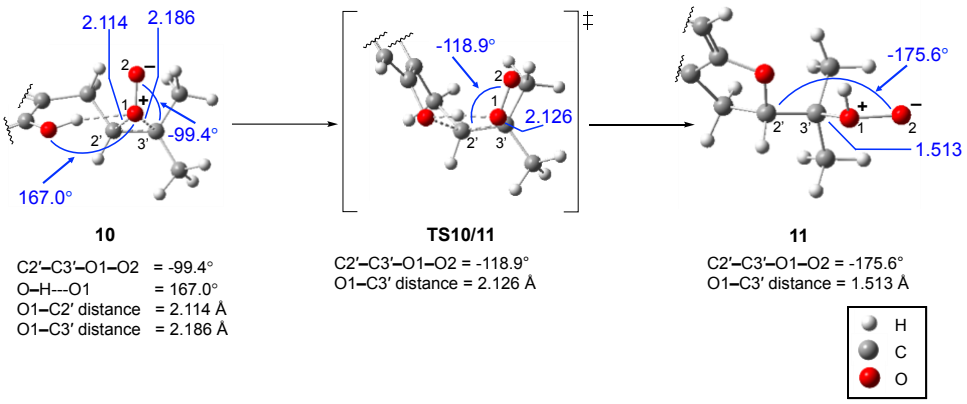


**Figure 7.** Path C: B3LYP/D95(d,p) calculation results show phenol hydrogen-bonding in the orthogonal orientation of the O1=O2 relative to the C2′–C3′ bond in **10**, and nearly parallel in the *iso*-hydroperoxide **11**.

**Path D with Dehydration to Reach Dihydrobenzofuran 9.** We focused on the bimolecular epoxidation reaction (path D in Figures 3 and 5). We have located a transition state (**TS11′/13**) on the potential energy surface (PES) for the O-transfer reaction of *iso*-hydroperoxide **11′** [2-(tetrahydrofuran-2-yl)propan-2-*iso*-hydroperoxide] to 2-methyl-2-butene **13**. Transition structure **TS11′/13** was found with an activation energy of 1.1 kcal/mol, in which the smaller molecules **11′** and **13** were used due to the prohibitively large size to compute the glycocitrine *iso*-hydroperoxide **6** with the prenyl group of a second glycocitrine molecule. In **TS11′/13**, the structure bears O2···C11 and O2···C12 bond distances of 2.440 Å and 2.455 Å, respectively. The

reaction of **11′** and **13** is exothermic by 86.9 kcal/mol with B3LYP/D95(d,p) and 93.0 kcal/mol with M062X/6-31+G(d,p) calculations to reach abbreviated compounds to the corresponding epoxide **7** and alcohol **8**. An additional step would be needed to reach elimination product **9**, which is rationalized by alcohol **3** in a dehydration step to furnish **9**, although a unimolecular path (path E) to **9** is also found.

**Path E to Dihydrobenzofuran 9.** The formation of **9** can arise by $H_2O_2$ cleavage from *iso*-hydroperoxide **11** via **TS11/9**. The activation barrier of **TS11/9** is 5.9 kcal/mol, where the transition state has an O–C bond distance of 1.524 Å and H–O1–O2–H dihedral angle of 94.7°, thereby releasing $H_2O_2$. An 90° angle is preferred for free HOOH, where dihedral angle increases lead to enhanced lone-pair interactions on adjacent oxygen atoms. This is known to be destabilizing from antibonding overlap in the $\pi^*$ molecular orbital, which can reduce the oxygen-oxygen bond energy. Since the activation barrier to **9** in path C is higher than **TS11′/13** in path D, path D is suggested to be concentration dependent in **6**. The participation of *iso*-hydroperoxide **11** is reasoned based on two paths to **9**, in addition to conversion to a conventional hydroperoxide **12** (path F).

**Path F to Hydroperoxide 12.** Our computed data predict the formation of **12**, but in a slightly higher energy path F via **TS11/12** (6.7 kcal/mol) compared to path D (1.1 kcal/mol) and path E (5.9 kcal/mol). In comparison to *iso*-hydroperoxide **11**, the corresponding hydroperoxide **12** has a shorter O1–O2 bond distance by 0.04 Å and a shorter O1–C3′ bond distance by 0.061 Å. Similar to our 7.3 kcal/mol computed barrier in path F, Meredith et al. (29) computed a barrier of 5.7 kcal/mol in oxywater ($H_2O^+$–$O^-$) to reach HOOH. The proton affinity of **11** of 322.4 kcal/mol is on par or slightly lower than typical organic acids, suggesting that proton transfer to reach **12** can also arise through the loss and gain of the proton by the surrounding medium.

**Mechanistic Summary.** Here, mechanistic facets are summarized in which (i) glycocitrine curvature from the *N*-methyl distorts its phenol ring bringing the OH group and the prenyl group closer together, (ii) $^1O_2$ oxidation of glycocitrine leads to an *iso*-hydroperoxide whose structure bears similarity to other *iso* species, and (iii) pincer action which enhances the protic environment at glycocitrine's prenyl group.

(i) The DFT results in Table 1 show that the prenyl phenol **1** has a longer O–H···C2′ bond and nearly flat phenol ring, whereas glycocitrine **6** has a shorter O–H···C2′ bond and puckered phenol bringing the OH and prenyl groups closer together. The O–H···C2′ in **6** is shorter than **1** by ~0.13 Å. The dihedral angle ϕ for phenol in **6** (C1a–C4a–C4–C3) is puckered by ~9.1° compared to the nearly flat phenol in **1** (C4–C3–C2–C1) = 1.0°. The proximity of the OH and prenyl groups are also reduced as judged by θ for **6** C3–C4–C1′–C2′ that is increased by ~11-16° compared to θ for **1** C1–C2–C1′–C2′; and δ for **6** C1a–C4a–C4–C1′ that is increased by ~11-13° compared to δ for **1** C4–C3–C2–C1′.

**Table 1.** Computed structure comparisons of prenyl phenol **1** and glycocitrine **6**

| Compound | model chemistry/basis set | | | |
|---|---|---|---|---|
| | B3LYP/d95(d,p) and (in parentheses for M062X/6-31+G(d,p)) | | | |
| | O–H···C2′ bond distance | ϕ | θ | δ |
| 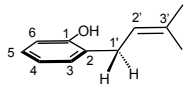 prenyl phenol **1** | 2.15 Å (2.26 Å) | 1.0° (1.0°) | 54.5° (61.6°) | 176.8° (177.9°) |
| 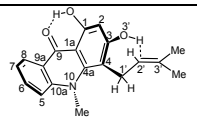 glycocitrine **6** | 2.03 Å (2.11 Å) | 9.1° (9.3°) | 43.7° (45.4°) | 166.2° (164.8°) |

Dihedral angle ϕ: for **1** C4–C3–C2–C1; for **6** C1a–C4a–C4–C3.

Dihedral angle θ: for **1** C1–C2–C1′–C2′; for **6** C3–C4–C1′–C2′.

Dihedral angle δ: for **1** C4–C3–C2–C1′; for **6** C1a–C4a–C4–C1′.

The DFT results in Table 2 suggest that the fate of glycocitrine **6** from $^1O_2$ oxidation is also linked to the reduced curvature in the products. For example, the dihedral angle ε (C4–C4a–N10–C10a) in **6** is increased by ~0.3-4.7° compared to products **9**-**7**, and **12**. In terms of product formation, notice the O-transfer reaction to a second prenyl group leads to an epoxide **7** and alcohol **8** (Figures 3 and 5, path D). Higher concentrations of glycocitrine **6** would be expected to undergo bimolecular path D with formation of the dihydrofuran **9** until the concentration of **6** is exhausted, at which point a unimolecular paths (paths E and F) can compete. Because glycocitrine **6** possesses

a pyramidal *N*-methyl group and phenol intramolecular H-bonding similar to other prenylated natural products that can form dihydrobenzofurans (3-10), the *iso*-hydroperoxide may represent a key intermediate in natural products biosynthesis.

**Table 2.** Computed structure of glycocitrine **6** and reaction products

| **compound** | **model chemistry/basis set** |
|---|---|
| | B3LYP/D95(d,p) and (in parentheses for M062X/6-31+G(d,p)) |
| | ε C4–C4a–N10–C10a |
| glycocitrine **6** | 162.7° (162.8°) |
| epoxide **7** | 163.0° (163.6°) |
| alcohol **8** | 167.0° (165.7°) |
| dihydrobenzofuran **9** | 167.4° (165.9°) |
| hydroperoxide **12** | 167.1° (165.8°) |

(ii) The *iso*-hydroperoxide displays somewhat similar structural features to *iso*-iodoform (*iso*-$CHI_2^+$–$I^-$). For *iso*-hydroperoxide **11**, our calculations show an O1–O2 distance of 1.492 Å and C3′–O1–O2 angle of 113.0°, whereas *iso*-iodoform possesses an I–I distance of 2.92 Å and C–I–I angle 133.9° (30). However, the *iso*-hydroperoxide is dissimilar to other *iso* intermediates. For example, the photoisomerization of $BiI_3$ to *iso*-$BiI_2$–I is also accompanied by dissociation to $BiI_2^{\bullet}$ and $I^{\bullet}$ radicals, which recombine to form ground-state $BiI_3$ and $I_2$ based on time-resolved X-ray liquidography and DFT calculations (35). Furthermore, $CHBr_3$ can form *iso*-$CHBr_2^+$–$Br^-$, and

$CHI_3$ can form *iso*-$CHI_2^+$–$I^-$ based on transient IR spectroscopy (31), as well as femtosecond pump−probe spectroscopy and nanosecond laser flash photolysis (31). Additionally dissimilar to *iso*-hydroperoxide, the $CH_2I^+$−$I^-$ and $CHI_2^+$−$I^-$ isomers formed by photoisomerizations of $CH_2I_2$ and $CHI_3$ can transfer methylene and iodomethylene groups to alkenes forming cyclopropanes (32), although in our case *iso*-hydroperoxide can serve as an epoxidizing agent. We also note that the *iso*-hydroperoxide is structurally reminiscent of carbonyl oxides ($R_2C{=}O^+{-}O^-$) formed in the reaction of carbenes and oxygen (36-38). Figure 8 shows computed electrostatic potential maps for the model systems *iso*-hydroperoxy-2-methylpropane (**14**) and 2-carbonyloxypropane (**15**) are similar except for the deficiency of electron density (blue) at the oxonium ion of **14**. The structures are also quite similar; **14** has an O1–O2 distance of 1.466 Å and C3′–O1–O2 angle of 112.8°, and **15** has an O1–O2 distance of 1.371 Å and C3′–O1–O2 angle 117.2°.

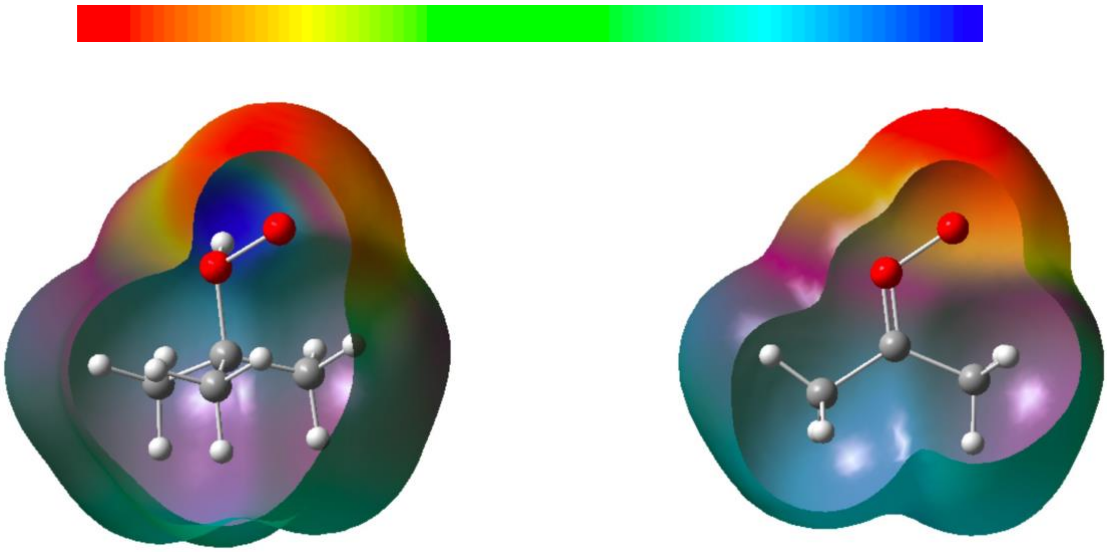


**Figure 8.** Computed electrostatic potential maps for model compounds *iso*-hydroperoxy-2-methylpropane (**14**) and 2-carbonyloxypropane (**15**). The electron-density isosurface value was set at 0.0004 au and a portion of the front-facing image removed for a view of the interior of the molecule. Colors of the map potentials range from red (negative) to green (neutral) to blue (positive).

(iii) Our calculated results point to the existence of a phenol O–H···π prenyl in glycocitrine **6**. Similar O–H···π hydrogen bonds between alcohols and alkenes have been reported (39). For example, *syn*-7-norbornenol bears an O–H···π interaction with a distance of 1.97 Å and is stabilized by 7.3 kcal/mol due to this hydrogen bond (40). MP2 calculations also showed an O–H···π bond between benzene and water also show an attractive interaction of 3.2 kcal/mol (41), and a preferred intramolecular O–H···π conformation in homoallylic alcohols, such as of epicholesterol (42). In the case of glycocitrine **6**, the soft O–H···π prenyl bond is enhanced due to distortion imposed by the remote *N*-methyl group. The computed approach of $^1O_2$ to the prenyl

group favors a T-shape relative to the allylic π cloud. Calculations using a start-guess structure with the approach of $^1O_2$ to the prenyl group in a parallel fashion converted to a T-shape upon optimization (Figure S1, Supporting Information). Thus, the O–H···$^1O_2$ hydrogen bonding appears to facilitate the formation of the *iso*-hydroperoxide **11**. Steering effects of $^1O_2$ by hydroxy groups have been reported and can lead to shallow minima, in which the presence of a water interface (20) perturb the 'ene' reaction. The reaction of $^1O_2$ with simple alkenes such as tetramethylethylene leads to a perepoxide transition state (25), that can convert to a minimum in a distorted structure (e.g., *trans*-cyclooctene) (24) or to a resonance-stabilized zwitterionic peroxy intermediate (e.g., heptamethine cyanine) (21,43). The reaction of $^1O_2$ with prenyl phenols, prenylsurfactants, and prenyllipids can arise by 'ene' reactions (44-47), where our current results expand on the topic by implicating intramolecular H-bonding in the reaction of $^1O_2$ with **6** and the formation of an *iso*-hydroperoxide intermediate.

**Conclusion**

The work reveals–for the first time–theoretical evidence of an *iso*-hydroperoxide intermediate [R(H)$O^+$–$O^-$] in the formation of a natural product, in this case a natural dihydrobenzofuran. The formation of the *iso*-hydroperoxide intermediate is facilitated by the 16° curvature of the acridone ring and phenol/prenyl O–H···π bonding. Our theoretical evidence for the *iso*-hydroperoxide intermediate can be potentially impactful to the fields of biomimetic $^1O_2$ chemistry for biasing the path away from the 'ene' reaction. Future mechanistic studies could focus on nanoparticle surface hydrophobicity to conceivably enhance the *iso*-hydroperoxide and the dihydrobenzofuran formation. Alternate routes to the *iso*-hydroperoxide are conceivable, where future studies could focus on the reaction of O($^3$P) atoms (48,49) with alcohols to reach *iso*-

hydroperoxide, for a potentially similar reaction of $H_2O$ with $O(^3P)$ to reach oxywater [$H_2O^+$–$O^-$] (50).

**Theoretical Section**

The Gaussian16 program (revision C.01) was used to conduct calculations (51). B3LYP/D95(d,p) and M062X/6-31+G(d,p) calculations were carried out. Here, reaction enthalpies are provided which include thermal (298 K) and zero-point energy corrections using standard procedures (52,53). We find that B3LYP performs reasonably well in comparison with M062X. Stationary points of intermediates **16-18** from B3LYP/D95(d,p) and M062X/6-31+G(d,p) calculations are similar, for example, the hydrogen bonds are within 0.009-0.053 Å and the C4–C4a–N10–C(Me) dihedral angles are within 0.1-2.9° of each other (Supporting Information). To compute the approach of $^1O_2$ to the prenyl group of **6**, energies were computed and compared at constrained distances ranging from 1.0 to 3.0 Å, in which **10** is found to reside in a shallow minimum courtesy of the intramolecular phenol H-bond, where absence of this H-bond leads to a saddle point and bifurcation on the PES. The energetic values at this part of the PES (**6** + $^1O_2$ → **10**) are less reliable due to the multi-reference character of the wave function. T1 values were computed to determine whether spin contamination presented problems. T1 diagnostics can show that contamination is problematic if they are ≥0.02 for closed-shell systems or ≥0.03 for open-shell systems. In Table 3, we find that spin contamination does not appear to be problematic, based on DLPNO-CCSD(T)/aug-cc-pVTZ/C calculations with T1 values ranging from 0.011 to 0.014. Larger T1 values would have pointed to non-dynamical correlation or problematic multiconfigurational effects. Stationary points were also analyzed by vibrational frequency calculations. Verification of transition structures was carried out by tracing their internal reaction

coordinates (IRC) and by analysis of frequency calculations. Natural bonding orbital (NBO) calculations were carried out to quantify the H-bonding between $^1O_2$ and the phenol OH using NBO 7.0 (54,55). B3LYP/D95(d,p) polarized continuum model (PCM) water solvation calculations predict that the barrier heights are higher by relatively small amounts (1.3-3.0 kcal/mol) and reaction exothermicities reduced by fairly small quantities (0.3-5.4 kcal/mol). The above calculations were carried out for singlet channels; calculations of the triplet channels for diradicals were found to be ~13-57 kcal/mol higher in energy (Table S1, Supporting Information). The energy of $^1\Delta_g$ oxygen used was from the experimental singlet–triplet gap of 22.5 kcal/mol, which was added to the value computed for $^3\Sigma_g^+$ oxygen.

**Table 3.** T1 diagnostic values of prenyl phenol/$^1O_2$ intermediates and products.

| DFT method/basis set | intermediates and products | | |
|---|---|---|---|
| | 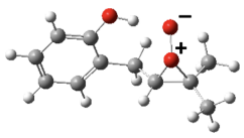 perepoxide **16** | 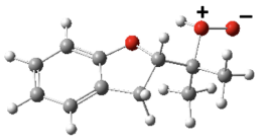 *iso*-hydroperoxide **17** | 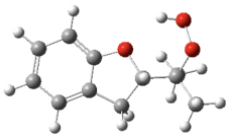 hydroperoxide **18** |
| B3LYP/d95(d,p) | 0.0140 | 0.0121 | 0.0107 |
| M062X/6-31+G(d,p) | 0.0141 | 0.0121 | 0.0106 |

**Acknowledgements**

We thank the National Science Foundation (CHE-2154133) for funding. A.M.D. also acknowledges support from a Fulbright-CONICET fellowship. This work used Comet and

Expanse, in the Extreme Science and Engineering Discovery Environment (XSEDE) cluster and Advanced Cyberinfrastructure Coordination Ecosystem: Services & Support (ACCESS) at the San Diego Supercomputer Center, which is supported by the NSF (ACI-1548562) through allocation CHE-210052. We thank Leda Lee for the graphic arts work.

**Supporting Information**

Supporting Information is available, which includes:

Energies and Cartesian Coordinates of structures at B3LYP/D95(d,p)

Energies and Cartesian Coordinates of structures at M062X/6-31+G(d,p)

Figure S1. M062X/6-31+G(d,p) computed start-guess structure **A** that optimizes to **B**

Table S1. Computed singlet and triplet energies of intermediates and products

Table S2. Second order perturbation theory analysis of Fock matrix in NBO basis

**ORCID**

Lloyd Lapoot: 0000-0001-6888-2626

Shakeela Jabeen: 0000-0002-7153-3379

Andrés M. Durantini: 0000-0002-7898-4033

Alexander Greer: 0000-0003-4444-9099

## References


1. Jabeen, S., G. Ghosh, L. Lapoot, A. M. Durantini, and A. Greer (2023) Sensitized photooxidation of *ortho*-prenyl phenol: Biomimetic dihydrobenzofuran synthesis and total $^1O_2$ Quenching. *Photochem. Photobiol.* **99**, 637–641.
2. Tang, M. C., Y. Zou, K. Watanabe, C. T. Walsh, and Y. Tang (2017) Oxidative cyclization in natural product biosynthesis. *Chem. Rev.* **117**, 5226–5333.
3. Singh, I. P., J. Sidana, S. B. Bharate, and W. J. Foley (2010) Phloroglucinol compounds of natural origin: Synthetic aspects. *Nat. Prod. Rep.* **27**, 393–416.
4. Ciochina, R., and R. B. Grossman (2006) Polycyclic polyprenylated acylphloroglucinols. *Chem. Rev.* **106**, 3963–3986.
5. Singh, I. P., and S. B. Bharate (2006) Phloroglucinol compounds of natural origin. *Nat. Prod. Rep.* **23**, 558–591.
6. Grundon, M. F., W. Probst, and J. Reisch (1990) Natural product chemistry, part 132: Synthesis and oxidative cyclisation of 1,3-dihydroxy-10-methyl-4-(3-methylbut-2-enyl)-9(10*H*)-acridinone (Glycocitrine-II). *Monatsh. Chem*. **121**, 157–163.
7. Ito, C., T. Ono, K. Hatano, and H. Furukawa (1993) Oxidation of glycocitrine-II. One of the *o*-prenylated phenolacridone alkaloids, with *m*-chloroperbenzoic Acid. *Chem. Pharm. Bull.* **41**, 383–385.
8. Funayama, S., and G. A. Cordell (1985) Chemistry of acronycine IX. Formation of dimers of noracronycine-mechanistic studies. *J. Nat. Prod.* **48**, 547–554.
9. Griesbeck, A. G., M. Bräutigam, M. Kleczka, and A. Raabe (2017) Synthetic approaches to mono- and bicyclic perortho-esters with a central 1,2,4-trioxane ring as the privileged lead structure in antimalarial and antitumor-active peroxides and clarification of the peroxide relevance. *Molecules* **22**, 119.
10. Ghogare, A. A. and A. Greer (2016) Using singlet oxygen to synthesize natural products and drugs. *Chem. Rev.* **116**, 9994–10034.

11. Montagnon, T., D. Noutsias, I. Alexopoulou, M. Tofi, and G. Vassilikogiannakis (2011) Green oxidations of furans—initiated by molecular oxygen—that give key natural product motifs. *Org. Biomol. Chem.* **9**, 2031–2039.
12. Griesbeck, A. G., L. O. Höinck, and J. M. Neudörfl (2010) Synthesis of spiroannulated and 3-arylated 1,2,4-trioxanes from mesitylol and methyl 4-hydroxytiglate by photooxygenation and peroxyacetalization. *Beilstein J. Org. Chem*. **6**, 61.
13. Alberti, M. N. and M. Orfanopoulos (2010) Recent mechanistic insights in the singlet oxygen ene reaction. *Synlett* **7**, 999–1026.
14. Montagnon, T., M. Tofi, and G. Vassilikogiannakis (2008) Using singlet oxygen to synthesize polyoxygenated natural products from furans. *Acc. Chem. Res.* **41**, 1001–1011.
15. Adam, W., N. Bottke, O. Krebs, I. Lykakis, M. Orfanopoulos, and M. Stratakis (2002) Ene reaction of singlet oxygen, triazolinedione, and nitrosoarene with chiral deuterium-labeled allylic alcohols: The interdependence of diastereoselectivity and regioselectivity discloses mechanistic insights into the hydroxy-group directivity. *J. Am. Chem. Soc.* **124**, 14403–14409.
16. Dussault, P. H., and J. A. Schultz (1999) Diastereoselective addition of singlet oxygen to highly functionalized *z*-allylic alcohols: Effect of neighboring functional groups. *J. Org. Chem.* **64**, 8419–8422.
17. Linker, T., and L. Froehlich (1995) Substituent effects in the highly regioselective and diastereoselective ene reaction of singlet oxygen with chiral cyclohexadienes. *J. Am. Chem. Soc.* **117***,* 2694–2697.
18. Adam, W., and H. G. Brünker (1993) Diastereoselective and regioselective photooxygenation of a chiral allylic amine and its acyl derivatives: Stereochemical evidence for a steering effect by the amino group in the ene reaction of singlet oxygen. *J. Am. Chem. Soc.* **115**, 3008–3009.

19. Clennan, E. L., X. Chen, and J. J. Koola (1990) Steric and electronic effects on the conformations and singlet oxygen ene regiochemistries of substituted tetramethylethylenes. The origin of the geminal effect. *J. Am. Chem. Soc.* **112**, 5193–5199.

20. Malek, B., W. Lu, P. P. Mohapatra, N. Walalawela, S. Jabeen, J. Liu, and A. Greer (2022) Probing the transition state-to-intermediate continuum: Mechanistic distinction between a dry vs wet perepoxide in the singlet oxygen 'ene' reaction at the air-water interface. *Langmuir* **38**, 6036-6048.

21. Matikonda, S. S., D. A. Helmerich, M. Meub, G. Beliu, P. Kollmannsberger, A. Greer, M. Sauer, and M. J. Schnermann (2021) Defining the basis of cyanine phototruncation enables a new approach to single molecule localization microscopy. *ACS Cent. Sci.* **7**, 1144-1155.

22. Griesbeck, A. G., B. Goldfuss, C. Jäger, E. Brüllingen, T. Lippold, and M. Kleczka (2017) Strong asymmetry in the perepoxide bifurcation mechanism: The large-group effect in the singlet oxygen ene reaction with allylic alcohols. *ChemPhotoChem* **1**, 213–221.

23. Sheppard, A. N., and O. Acevedo (2009) Multidimensional exploration of valley−ridge inflection points on potential-energy surfaces. *J. Am. Chem. Soc.* **131**, 2530–2540.

24. Leach, A. G., K. N. Houk, and C. S. Foote (2008) Theoretical prediction of a perepoxide intermediate for the reaction of singlet oxygen with *trans*-cyclooctene contrasts with the two-step no-intermediate ene reaction for acyclic alkenes. *J. Org. Chem*. **73**, 8511– 8519.

25. Singleton, D. A., C. Hang, M. J. Szymanski, M. P. Meyer, A. G. Leach, K. T. Kuwata, J. S. Chen, A. Greer, C. S. Foote, and K. N. Houk (2003) Mechanism of ene reactions of singlet oxygen. A two-step no-intermediate mechanism. *J. Am. Chem. Soc.* **125**, 1319–1328.

26. Garavelli, M., F. Bernardi, M. Olivucci, and M. A. Robb (1998) DFT study of the reactions between singlet oxygen and a carotenoid model. *J. Am. Chem. Soc.* **120**, 10210–10222.

27. Li, J., and J. Li (2021) A full-dimensional potential energy surface and dynamics of the multichannel reaction between H and $HO_2$. *J. Phys. Chem. A* **125**, 1540–1552.

28. Huang, H. H., Y. Xie, and H. F. Schaefer (1996) Can oxywater be made? *J. Phys. Chem.* **100**, 6076–6080.

29. Meredith, C., T. P. Hamilton, and H. F. Schaefer (1992) Oxywater (water oxide): New evidence for the existence of a structural isomer of hydrogen peroxide. *J. Phys. Chem.* **96**, 9250–9254.

30. Ahn, C. W., H. Ki, J. Kim, S. Park, Y. Lee, K. H. Kim, Q. Kong, J. Moon, M. N. Pedersen, M. Wulff, and H. Ihee (2018) Direct observation of a transiently formed isomer during iodoform photolysis in solution by time-resolved x-ray liquidography. *J. Phys. Chem. Lett.* **9**, 647–653.

31. Preston, T. J., M. A. Shaloski, and F. F. Crim (2013) Probing the photoisomerization of $CHBr_3$ and $CHI_3$ in solution with transient vibrational and electronic spectroscopy. *J. Phys. Chem. A* **117**, 2899–2907.

32. Tarnovsky, A. N., I. Pascher, and T. Pascher (2007) Reactivity of *iso*-diiodomethane and *iso*-iodoform, isomers of $CH_2I_2$ and $CHI_2$, toward the double bond of a variety of cycloalkenes. *J. Phys. Chem. A* **111**, 11814–11817.

33. Wall, M., A. N. Tarnovsky, T. Pascher, V. Sundström, and E. Åkesson (2003) Photodissociation dynamics of iodoform in solution. *J. Phys. Chem. A* **107**, 211–217.

34. Skraba-Joiner, S. L., J. W. Brulet, M. K. Song, and R. P. Johnson (2017) Acid-catalyzed skeletal rearrangements in arenes: Aryl versus alkyl ring pirouettes in anthracene and phenanthrene. *J. Org. Chem.* **82**, 13076–13083.

35. Choi, E. H., D. S. Ahn, S. Park, C. Kim, C. W. Ahn, S. Kim, M. Choi, C. Yang, T. W. Kim, H. Ki, J. Choi, M. N. Pedersen, M. Wulff, J. Kim, and H. Ihee (2019) Structural

dynamics of bismuth triiodide in solution triggered by photoinduced ligand-to-metal charge transfer. *J. Phys. Chem. Lett.* **10**, 1279–1285.

36. Tomioka, H. (2004) Triplet carbenes. In: *Reactive Intermediate Chemistry* (Edited by R. A. Moss, M. S. Platz and M. Jones Jr.) pp. 424-429. Hoboken, NJ: John Wiley & Son, Ltd.
37. Sander, W., G. Bucher and S. Wierlacher (1993). Carbenes in matrixes: spectroscopy, structure, and reactivity. *Chem. Rev.* **93***,* 1583–1621.
38. Sawwan, N. and A. Greer (2007) Rather exotic types of cyclic peroxides: Heteroatom dioxiranes. *Chem. Rev.* **107**, 3247–3285.
39. Heger, M., R. A. Mata, and M. A. Suhm (2015) Soft hydrogen bonds to alkenes: The methanol–ethene prototype under experimental and theoretical scrutiny. *Chem. Sci.* **6**, 3738–3745.
40. Struble, M. D., M. G. Holl, G. Coombs, M. A. Siegler, and T. Lectka (2015) Synthesis of a tight intramolecular OH···olefin interaction, probed by IR, $^{1}$H NMR, and quantum chemistry. *J. Org. Chem.* **80**, 4803–4807.
41. Tsuzuki, S., K. Honda, T. Uchimaru, M. Mikami, and K. Tanabe (2000) Origin of the attraction and directionality of the NH/π interaction: Comparison with OH/π and CH/π interactions. *J. Am. Chem. Soc.* **122**, 11450–11458.
42. Bakke, J. M., and L. H. Bjerkeseth (1988) The Conformational composition of 3-buten-1-ol, the importance of intramolecular hydrogen bonding. *J. Mol. Struct.* **470**, 247–263.
43. Turque, O., A. Greer, and O. R. Wauchope (2020) Synthetic feasibility of oxygen-driven photoisomerizations of alkenes and polyenes. *Org. Biomol. Chem.* **18,** 9181-9190.
44. Griesbeck, A. G., M. Kleczka, A. de Kiff, M. Vollmer; A. Eske, and S. Sillner (2015) Singlet oxygen and natural substrates: Functional polyunsaturated models for the photooxidative degradation of carotenoids. *Pure Appl. Chem.* **87**, 639–647.
45. Griesbeck, A. G., W. Adam, A. Bartoschek, and T. El-Idreesy (2003) Photooxygenation of allylic alcohols: Kinetic comparison of unfunctionalized alkenes with prenol-type allylic alcohols, ethers, and acetates. *Photochem. Photobiol. Sci.* **2**, 877–881.

46. Helesbeux, J. J., O. Duval, C. Dartiguelongue, D. Séraphin, J. M. Oger, and P. Richomme (2004) Synthesis of 2-hydroxy-3-methylbut-3-enyl substituted coumarins and xanthones as natural products. Application of the Schenck ene reaction of singlet oxygen with *o*-prenyl phenol precursors. *Tetrahedron* **60**, 2293–2300.

47. Gruszka, J., A. Pawlak, and J. Kruk (2008) Tocochromanols, plastoquinol, and other biological prenyllipids as singlet oxygen quenchers−Determination of singlet oxygen quenching rate constants and oxidation products. *Free Radic. Biol. Med.* **45**, 920–928.

48. Omlid, S. M., S. A. Dergunov, A. Isor, K. L. Sulkowski, J. T. Petroff, E. Pinkhassik, and R. D. McCulla (2019) Evidence for diffusing atomic oxygen uncovered by separating reactants with a semi-permeable nanocapsule barrier. *Chem. Commun.* **55**, 1706–1709.

49. Korang, J., W. R. Grither, and R. D. McCulla (2010) Photodeoxygenation of dibenzothiophene *S*-oxide derivatives in aqueous media. *J. Am. Chem. Soc.* **132**, 4466–4476.

50. Pehkonen, S., K. Marushkevich, L. Khriachtchev, M. Räsänen, B. L. Grigorenko, and A.V. Nemukhin (2007) Photochemical synthesis of $H_2O_2$ from the $H_2O\cdots O(^3P)$ van Der Waals complex: Experimental observations in solid krypton and theoretical modeling. *J. Phys. Chem. A* **111**, 11444–11449.

51. Frisch, M. J., G. W. Trucks, H. B. Schlegel, G. E. Scuseria, M. A. Robb, J. R. Cheeseman, G. Scalmani, V. Barone, G. A. Petersson, H. Nakatsuji, X. Li, M. Caricato, A. V. Marenich, J. Bloino, B. G. Janesko, R. Gomperts, B. Mennucci, H. P. Hratchian, J. V. Ortiz, A. F. Izmaylov, J. L. Sonnenberg, D. Williams-Young, F. Ding, F. Lipparini, F. Egidi, J. Goings, B. Peng, A. Petrone, T. Henderson, D. Ranasinghe, V. G. Zakrzewski, J. Gao, N. Rega, G. Zheng, W. Liang, M. Hada, M. Ehara, K. Toyota, R. Fukuda, J. Hasegawa, M. Ishida, T. Nakajima, Y. Honda, O. Kitao, H. Nakai, T. Vreven, K. Throssell, J. A. Montgomery Jr., J. E. Peralta, F. Ogliaro, M. J. Bearpark, J. J. Heyd, E. N. Brothers, K. N. Kudin, V. N. Staroverov, T. A. Keith, R. Kobayashi, J. Normand, K. Raghavachari, A. P. Rendell, J. C. Burant, S. S. Iyengar, J. Tomasi, M. Cossi, J. M.

Millam, M. Klene, C. Adamo, R. Cammi; J. W. Ochterski, R. L. Martin, K. Morokuma, O. Farkas, J. B. Foresman, and D. J. Fox. (2016) Gaussian 16 Revision C.01, Gaussian, Inc., Wallingford, CT.

52. Jensen, F. (2021) Computational Chemistry: The exciting opportunities and the boring details. *Isr. J. Chem.* **62**, e202100027.

53. Jensen, F. (2017) How large is the elephant in the density functional theory room? *J. Phys. Chem.* A **121**, 6104–6107.

54. Glendening, E. D., J, K. Badenhoop, A. E. Reed, J. E. Carpenter, J. A. Bohmann, C. M. Morales, P. Karafiloglou, C. R. Landis, and F. Weinhold (2018) *NBO 7.0.* Theoretical Chemistry Institute, University of Wisconsin, Madison.

55. Liakos, D. G., M. Sparta, M. K. Kesharwani, J. M. L. Martin and F. Neese (2015) Exploring the accuracy limits of local pair natural orbital coupled-cluster theory. *J. Chem. Theory Comput.* **11**, 1525-1539.

**FIGURE CAPTIONS**

**Figure 1.** The sensitized photooxidation of *ortho*-prenyl phenol **1** in ref. 1. Preferential addition of $^1O_2$ to the prenyl site was attributed to hydrogen bonding with the phenol OH group, causing a divergence away from the singlet oxygen 'ene' products **4** and **5** toward the dihydrobenzofuran **2** as the major product in benzene.

**Figure 2.** Schematic drawing of prenyl phenol **1** showing a flat benzene ring and longer internal O–H···π bond. Glycocitrine **6** curvature distorts its phenol ring bringing the OH group and the prenyl group together closer.

**Figure 3.** Proposed mechanism of $^1O_2$ oxidation of the prenyl group in the natural product glycocitrine **6**. Path A shows that the curved **6** accentuates an internal O–H···π bond [(*S*) amine shown; both stereoisomers accentuate this O–H···π bond]; path B is the $^1O_2$ oxidation and formation a H-bonded perepoxide **10**; path C is the formation of the *iso*-hydroperoxide **11**; path D is the epoxidation of another glycocitrine prenyl group by O-transfer from **11**; path E is formation of the dihydrobenzofuran **9** with the departure of $H_2O_2$; and path F is the rearrangement of the *iso*-hydroperoxide **11** to hydroperoxide **12**.

**Figure 4.** B3LYP/D95(d,p) optimized structures showing (A) the positions of the NMe group in **6** and **6b** as down and up, respectively, and (B) the soft O–H···π interaction of the phenol OH with the prenyl group in **6** and rotamer **6b**.

**Figure 5.** DFT calculated potential energy surface for the reaction of glycocitrine **6** with $^1O_2$. Gas-phase energetics are in kcal/mol, shown for B3LYP/D95(d,p), and in parentheses for M062X/6-31+G(d,p). Relative energies: **6** and **6′** are relative to each other; 2-(tetrahydrofuran-2-yl)propan-2-*iso*-hydroperoxide **11′** and 2-methyl-2-butene is relative to **7** and **8**; and **9** and **12** are relative to **11**.

**Figure 6.** M062X/6-31+G(d,p) computed structure of the phenol OH stabilizing incoming $^1O_2$ to the prenyl site of **6**. NBO analysis of the oxygen atoms (O1 and O2) lone pair electron ($lp_1$ and $lp_2$) interactions with the σ* antibonding orbital of the phenol O3′–H group.

**Figure 7.** Path C: B3LYP/D95(d,p) calculation results show phenol hydrogen-bonding in the orthogonal orientation of the O1=O2 relative to the C2′–C3′ bond in **10**, and nearly parallel in the *iso*-hydroperoxide **11**.

**Figure 8.** Computed electrostatic potential maps for model compounds *iso*-hydroperoxy-2-methylpropane (**14**) and 2-carbonyloxypropane (**15**). The electron-density isosurface value was set at 0.0004 au and a portion of the front-facing image removed for a view of the interior of the molecule. Colors of the map potentials range from red (negative) to green (neutral) to blue (positive).

**Figure S1.** M062X/6-31+G(d,p) computed start-guess structure **A** optimizes to **B**, which is the precursor to perepoxide **10**.

**TABLE CAPTIONS**

**Table 1.** Computed structure comparisons of prenyl phenol **1** and glycocitrine **6**.

**Table 2.** Computed structure of glycocitrine **6** and reaction products.

**Table 3.** T1 diagnostic values of prenyl phenol/$^1O_2$ intermediates and products.

**Table S1.** M062X/6-31+G(d,p) computed singlet and triplet energies (in kcal/mol) of intermediates and products.

**Table S2.** Second order perturbation theory analysis of Fock matrix in NBO basis